Appl. Phys. A 90, 159–163 (2008)
DOI: 10.1007/s00339-007-4245-9

Applied Physics A
Materials Science & Processing

M. MARTINEZ PACHECO[1]
R.H.B. BOUMA[2,✉]
L. KATGERMAN[1,3]

Combustion synthesis of TiB_2-based cermets: modeling and experimental results

[1] The Netherlands Institute for Metals Research, P.O. Box 5008, 2600 GA Delft, The Netherlands
[2] TNO Defense, Security and Safety, P.O. Box 45, 2280 AA Rijswijk, The Netherlands
[3] Materials Science and Engineering, Delft University of Technology, Delft, The Netherlands

Received: 5 February 2007/Accepted: 17 July 2007
Published online: 1 September 2007 •

ABSTRACT TiB_2-based cermets are prepared by combustion synthesis followed by a pressing stage in a granulate medium. Products obtained by combustion synthesis are characterized by a large remaining porosity (typically 50%). To produce dense cermets, a subsequent densification step is performed after the combustion process and when the reacted material is still hot. To design the process, numerical simulations are carried out and compared to experimental results. In addition, physical and electrical properties of the products related to electrical contact applications are evaluated.

PACS 81.20.Ka; 81.05.Mh; 72.80.Tm

1 Introduction

Self-propagating high-temperature synthesis (SHS), also known as combustion synthesis or solid-flame combustion, is considered a gasless combustion process. It is a cost-effective method for producing high-purity refractory compounds and advanced ceramics [1]. Here, the application to functionally graded cermets and electrical contact materials is shown.

The basis of the reaction synthesis relies on the ability of gasless and highly exothermic reactions to be self-sustaining. Ignition can be achieved by a laser beam, ohmic heating, induction, or spark. However, a sufficient amount of energy needs to be deposited for the reaction to become self-propagating. SHS has assumed significance for the production of intermetallics, ceramics, and cermets because it is a very rapid processing technique without the need for complex furnaces [2], and can increase the productivity in comparison with conventional techniques. One of the drawbacks of this technique is the high porosity of the final product (typically 50%), due to: (1) initial porosity in the reactant mixture, and (2) the higher density of the reaction products with respect to starting materials. A subsequent densification stage is needed, which is often hard to achieve in ceramic composite materials because they are highly deformation-resistant. However, one may take advantage of the ductile behavior when reaction products are still hot and apply techniques such as hot pressing, hot rolling, hot isostatic pressing, or shock waves to eliminate porosity. Combustion synthesis followed by quasi-isostatic pressing (QIP) in a granulate medium is the technique for removal of porosity studied here.

In the QIP technique, the particulate acts as a pressure-transmitting medium (PTM) and redistributes an initially applied axial load to create a stress profile similar to isostatic pressing [3–7]. The pressure distribution in the PTM has been discussed in a previous paper [8]. In addition, the PTM thermally isolates the sample, thereby minimizing cracking due to rapid cooling and keeping the temperature of the specimen for a longer time above the ductile-to-brittle transition temperature of the ceramic phase. In this study, numerical simulations of the heat flow from the reacted material to its surroundings are presented and will be compared with experimental results in order to know whether a sufficient time-window exists for the required densification step after the completed SHS process.

The rapid development of SHS has provided a good option for the fabrication of advanced materials [5, 9–12]. Powder metallurgical arcing contact materials are advanced composite materials used in medium and high current applications such as circuit breakers and switchgears [13]. The homogeneity of their microstructure is essential for the physical characteristics and the switching performance of the electrical contacts. The main requirements for an arcing contact electrical material include high electrical conductivity, elevated melting point, and high hardness. Silver refractory metals possess these characteristics and are ideal for working in high current applications. Usually, the steps of production of these materials are mixing, pressing, sintering, and in some cases infiltration with liquid silver or copper [14]. Unfortunately, the processing used to fabricate these materials is the major disadvantage due to the high cost of the final products. Electrical contact materials may be produced by SHS, and materials including TiB_2, TiC, or WC as a ceramic phase and Ag, Cu, or Al acting as a binder, can be synthesized.

2 Experimental procedure

Figure 1 shows the steps followed in the gasless combustion process to produce the cermets for the various applications. In addition, this combustion process is carried out in a thermal insulating medium that can trans-

✉ Fax: +31-15-2843997, E-mail: richard.bouma@tno.nl

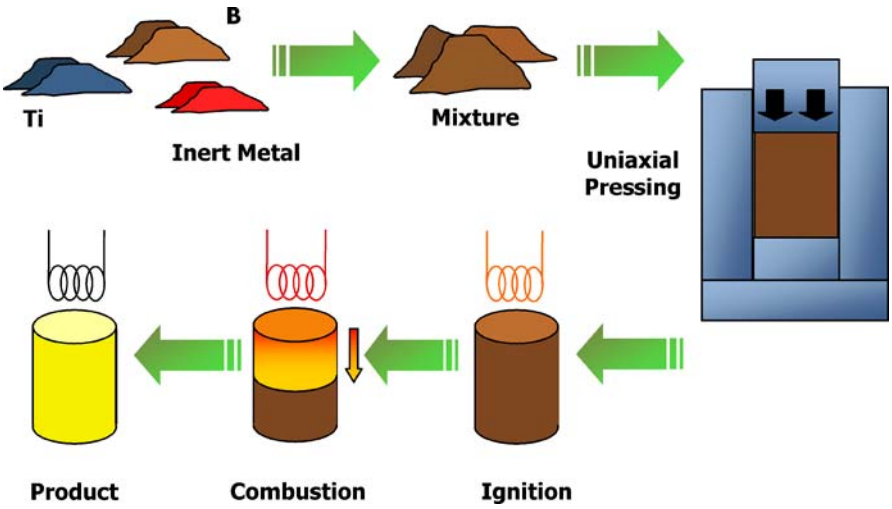

FIGURE 1 Scheme of the basic steps during the combustion synthesis process

fer the pressure for densification of the reacted and hot material.

As starting reactant materials, high-purity powders of amorphous boron (99.9%, average particle size of 1 μm, H.C. Starck), carbon (99.5%, 10 μm, Sigma Aldrich Chemie), and titanium (99.9% pure, 45 μm, Gimex Technische Keramiek) are used. As inert diluent materials a NiFe alloy with 50 wt % Fe and 50 wt % Ni (45 μm, H.C. Starck), copper powder (63 μm, Merck), and finally aluminium powder (45 μm, Mepura Metallpuver) are used in the experiments. High purity particles of alumina and carbon, with an average particle size of 45 μm, are used as constituents of the PTM. In order to fabricate electrical contact materials, stoichiometric mixtures of Ti and B are dry-mixed with 30 or 40 wt % of the inert metals copper or aluminium. The powders are uniaxially cold pressed in a steel die to 65%–75% TMD, obtaining cylindrical pellets with a diameter of 21 mm and thickness of about 15 mm.

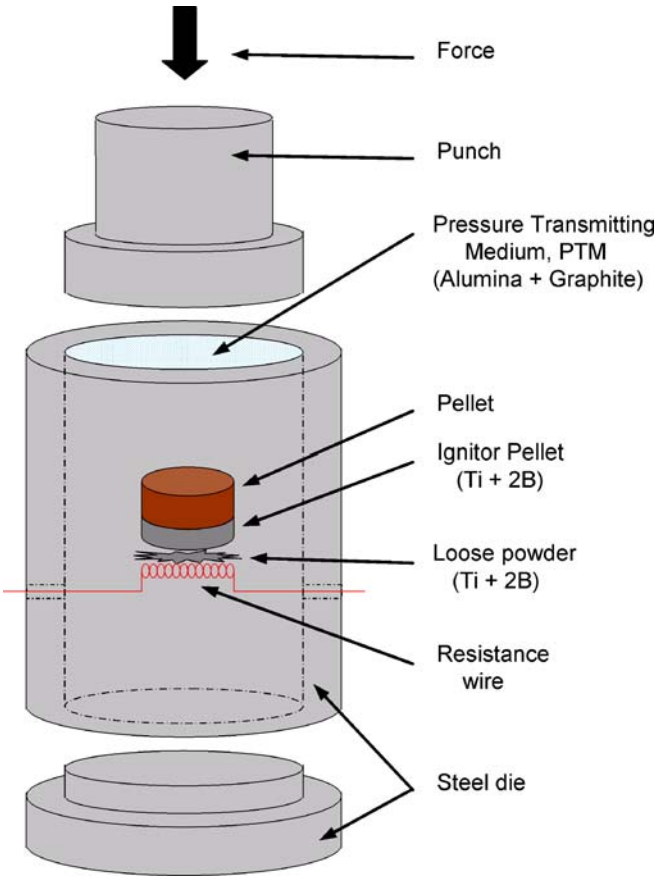

FIGURE 2 Schematic picture of the SHS/QIP setup for synthesis of electrical contact materials

Green pellets are placed in the loosely packed PTM (see detail in Fig. 2). In the case of functionally graded cermets, the side with the lowest metal content (5 wt %) is positioned at the bottom, in order to facilitate the ignition. The sample is ignited from below by a Kanthal coil through an ignitor pellet consisting of a titanium and boron stoichiometric mixture. This is a variation of Raman's technique [3], in which the hot PTM is poured on the green to ignite it. Experimentally it is observed that the SHS process is finished 3–6 s after ignition of the ignitor pellet. A pressure of 300–400 MPa is then applied 5–8 s after ignition, for a total duration of 100 s. Due to loading and unloading the press, maximum pressure is maintained for 50 s. After consolidation, the sample remains inside the die for slow cooling, avoiding cracking due to thermal stresses.

3 Theoretical calculations

The sustainability of a SHS reaction is closely related to the adiabatic or combustion temperature of the energetic mixture [15]. The combustion temperature T_c can be obtained from a heat balance equation supposing adiabatic conditions. In order to obtain accurate values of combustion temperature, the heat capacity as a function of the temperature, as well as the latent heat L at the melting and/or boiling point of the inert diluent, are introduced into the heat balance equation as follows:

$$\int X_P C_{pP}\,dT + \int X_D C_{pD}\,dT + \nu_1 X_D L_{s\to l} + \nu_2 X_D L_{l\to v} = Q(1 - X_D)\,, \quad (1)$$

where T is the temperature (K), C_{pP} and C_{pD} are the heat capacities ($J\,kg^{-1}K^{-1}$) of product and diluent respectively, Q is

	$T_{initial}$ °C	Conductivity $W(m\,K)^{-1}$	Density $kg\,m^{-3}$	Specific heat $J(kg\,K)^{-1}$	D_T $\times 10^{-5}\ m^2 s^{-1}$	$T_{melting}$ °C
Ignitor (TiB_2)	3200	25.92	4620	1222	0.46	3300
Sample (TiB_2-40 Cu)	2660	124.74*	6340	887.2	2.22	1080
Sample (TiB_2-40 Al)	2080	136.73*	3598.3	1089.2	3.49	660
Isolator (Al_2O_3 powder)	25	0.13**	1110	888.7	0.013	–

TABLE 1 Initial conditions and melting temperatures of the various materials and their thermal properties, conductivity, specific heat, and thermal diffusion coefficient

* Estimated from thermal conductivities of TiB_2 and Cu or Al
** Calculated from experimentally determined thermal diffusion coefficient of the pressure-transmitting medium

the heat of reaction ($J\,kg^{-1}$) with respect to the undiluted reactants, X_D is the mass fraction of diluent, and finally ν_1 and ν_2 represent the fraction of diluent that melts and/or evaporates, respectively.

In the experiments, a densification stage is added to the process to eliminate the remaining porosity in the final product. A time-window is predicted in which application of pressure is effective. It starts after completion of the SHS reaction in order not to quench the reaction and it ends with the solidification of the ceramic and/or metallic phase. This time-window for the QIP process can be determined either experimentally or numerically. Experimentally one may determine whether a good product density is obtained, with the disadvantage that several experiments are needed and for each individual configuration of the experiment.

Cooling down, after the gasless combustion process, has been simulated with the finite element code ABAQUS, which can solve heat transfer processes together with the effect of mechanical loads. Here an uncoupled thermal problem is considered initially, i.e., without the influence of the external applied pressure and without thermal stresses generated due to gradients in the system. The initial temperature of the reaction products corresponds to the calculated adiabatic reaction temperature, and the time to achieve the SHS reaction is not taken into account. Table 1 lists the thermal properties used in the simulations. A boundary condition of constant temperature is applied to the die wall.

To provide conductive heat transfer to the system, ABAQUS introduces a numeric gap conductance k that considers the effect of two closely adjacent (or contacting) surfaces on the conduction phenomenon. Simulations have been made considering both high and low values of k. Results have demonstrated that the gap conductance value is only relevant in the first moments of the cooling process (first 2 or 3 s). In this paper, results have been obtained considering an ideal contact between surfaces, and thus a high gap conductance value, which still allows a good approximation of the time-window for densification.

4 Results and discussion

4.1 *Experimental results*

Figure 3 shows the microstructure of a cross-section of a TiB_2-40 Cu cermet. The gray fraction represents the titanium diboride particles with a size below 10 μm. The red fraction corresponds to the copper phase, and black spots are remaining porosity. The microstructure appears refined and homogeneous. X-ray diffraction analysis shown in Fig. 4 indicates no formation of intermetallics in TiB_2-based cermets.

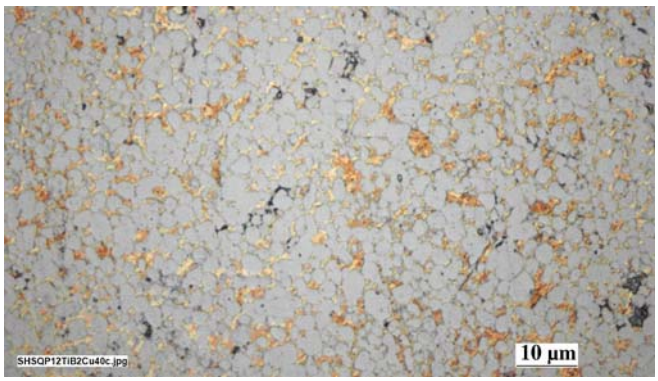

FIGURE 3 Optical micrograph of a TiB_2-xCu cermet with a 40 wt % Cu content

Table 2 lists the measured values of density, electrical conductivity, and Vickers hardness for TiB_2-based cermets. The relative density of the TiB_2 Al cermets is always higher than TiB_2 Cu cermets. The remaining porosity for the TiB_2-based materials with Al as a binder is reduced by only 2%. The large differences in final density for cermets with Cu or Al binder can be explained by the fact that the volume fraction of Al binder is larger than the volume fraction of Cu, providing an enhanced ductile behavior and hence facilitating the densification. Besides, Al has a lower melting point and remains longer in liquid state. The total energy release in the copper-based cermet is highest and it has been noticed that part of the copper is vaporized. The more violent reaction may explain an increase in porosity for cermets with Cu as an inert metal phase. Improvement of process parameters is needed to obtain high density TiB_2 Cu cermets.

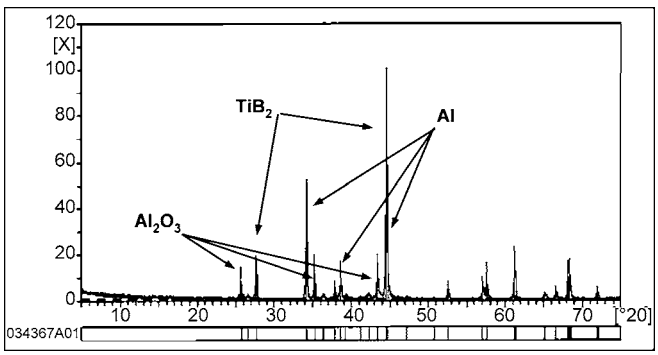

FIGURE 4 X-ray diffraction pattern of a TiB_2-40 Al cermet fabricated by combustion synthesis followed by quasi-isostatic pressing

Experiment No.	1	2	3	4	5	6	7	8	9
Metal content (vol%)	53% Al	26% Cu	53% Al	53% Al	26% Cu	26% Cu	42% Al	26% Cu	53% Al
Rel. density (% TMD)	87	65	98	92	58	60	91	56	95
σ ($\times 10^8$ $(\Omega\,\mathrm{m})^{-1}$)	0.155 ± 0.08	–	0.168 ± 0.08	0.139 ± 0.05	0.075 ± 0.03	0.037 ± 0.01	0.105 ± 0.04	0.023 ± 0.01	0.144 ± 0.05
HV (GPa)	2.81	3.93	3.48	3.63	4.27	4.78	3.52	4.45	3.78
$\varrho\sqrt{HV}$ ($\times 10^8\ \Omega\,\mathrm{m}\ (\mathrm{GPa})^{1/2}$)	1.10	–	1.11	1.37	2.77	5.84	1.59	9.19	1.35

TABLE 2 Measured density relative to theoretical maximum density (TMD), electrical conductivity σ, hardness value HV, and the parameter $\varrho\sqrt{HV}$ of TiB_2-based cermets obtained via SHS and QIP

In order to evaluate the properties of TiB_2-based cermets as materials for electrical contact applications, hardness and electrical conductivity need to be determined. Table 2 lists hardness values (HV) of TiB_2-xAl ($x = 53$ or 42 vol %) cermets ranging between 2.8 and 3.8 GPa. This rather low value as well as the large range is caused by the porosity of samples, making good hardness measurements a difficult task. The TiB_2-xAl samples show an electrical conductivity (σ) ranging between 1.4 and 1.7×10^7 $(\Omega\,\mathrm{m})^{-1}$, which is close to the calculated value for a fully dense sample of 2.3×10^7 $(\Omega\,\mathrm{m})^{-1}$. This value is comparable to that of some WC-40Ag contact materials fabricated by sintering and metal infiltration. In general a low resistivity is desired in electrical contact applications. The hardness of the material is equally important because of the moving and sometimes even sliding contact. The contact resistance, which is proportional to $\varrho\sqrt{HV}$ (with $\varrho = 1/\sigma$), is used as a design parameter for electrical contact materials. Values of $\varrho\sqrt{HV}$ have been determined and are also listed in Table 2.

4.2 *Theoretical calculations*

Sequences of the cooling process in TiB_2-40 Cu and TiB_2-40 Al cermets are shown in Fig. 5. One can observe that at 985 s the sample is still above 1000 °C, and that the thermal diffusion in the PTM is the rate-limiting step. When comparing the temperature profile at 0.9 s, one can see more or less homogeneous temperature distribution in the copper-based cermet, and steep temperature gradients in the aluminium-based cermet. This is due to the lower adiabatic reaction temperature for the aluminium-based cermet.

In Fig. 6, the temperature profiles at different locations and time-scales in sample and ignitor are shown. Within 10 s the temperature difference between ignitor and sample is equilibrated (see Fig. 7). This indicates that the thermal diffusion in the isolator is becoming the rate-limiting step and that one may take advantage of the heat in the ignitor to enhance the time-window of the QIP process. In Fig. 7, the melting temperature of copper is indicated and

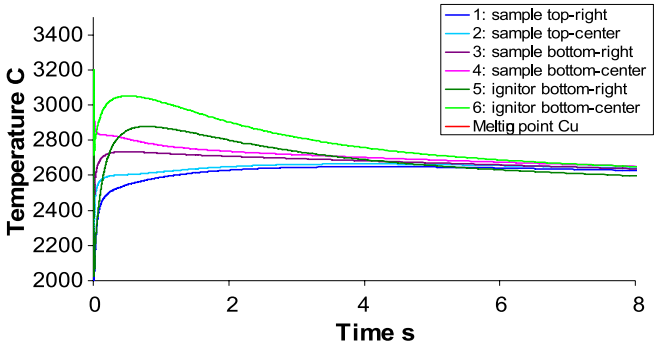

FIGURE 6 Temperature vs. time at indicated locations in sample and ignitor for TiB_2-40 Cu cermets

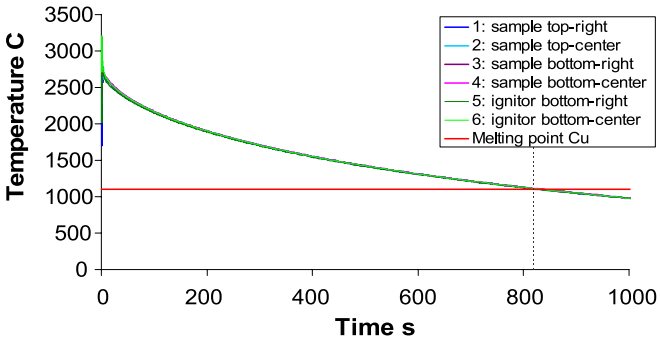

FIGURE 7 Temperature vs. time at indicated locations in sample and ignitor for TiB_2-40 Cu cermets, with expanded time-scale and melting indication of melting temperature of copper

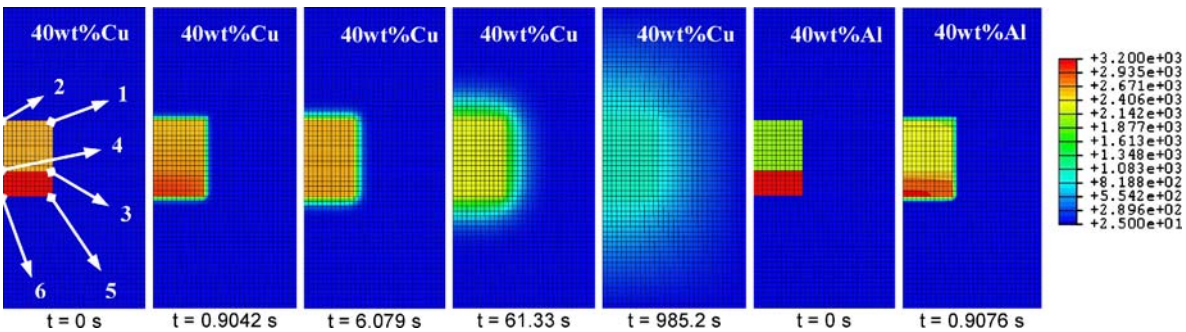

FIGURE 5 Evolution of the temperature profiles (temperature in °C and represented by different colors) for sample, ignitor, and isolator for TiB_2-40 Cu and TiB_2-40 Al cermets

the temperature in the SHS product drops below the melting temperature well after 800 s. Therefore, one may extend the experimentally applied time-window of only 100 s to 800 s. From the numerical simulations of the Al-based cermet an even longer time-window of 1350 s is calculated due to the lower melting temperature of aluminium with respect to copper.

5 Conclusions

TiB_2-based cermets for electrical contact applications with a 40 wt % of Cu and 30–40 wt % of Al have been prepared with SHS and a subsequent densification step in a granulate medium (QIP). The particulate transmits the initially applied axial load to the combustion synthesized sample when it is still hot and hence ductile. In addition to this, the time-window for densification for the various cermets has been theoretically simulated with the finite element code ABAQUS.

X-ray diffraction results indicated no formation of intermetallics that could weaken the microstructure. The remaining porosity of cermets with Cu is about 40%, while for cermets with Al it is only about 5%. This large difference is caused by the larger volume fraction of Al and its lower melting point.

The experimentally applied time-window was sufficient for densification of the TiB_2-40 Al. However, it is observed that the time-window for TiB_2 cermets with Cu binder was not sufficient.

Simulations with ABAQUS do indicate that, in all cases, the experimental time-window may be increased in order to achieve a better densification. Furthermore, the synthesis of cermet materials by SHS and QIP does benefit from the heat released by, e.g., a purely Ti + B mixture enlarging the time-window for the densification step.

The application of pressure is anticipated to decrease to some extent the time-window for densification due to compaction of the isolator, leading to a higher thermal diffusion coefficient in this material. This effect has not been taken into account in the numerical simulation.

REFERENCES

1 B.B. Khina, D.N. Loban, Modeling SHS in porous systems using cellular automata approach, in International Conference on Modeling and Simulation of Metal Technologies, MMT-2000, Ariel, Israel, November 13–15, 2000, pp. 412–418
2 J.B. Holt, in *Engineered Materials Handbook*, *Ceramics and Glasses* vol. 4, ed. by S.J. Schneider Jr. (ASM International, Materials Park, OH, 1991), pp. 227–231
3 R.V. Raman, S.V. Rele, S. Poland, J. LaSalvia, M.A. Meyers, A.R. Niiler, J. Metals. **3**, 23 (1995)
4 Z.Y. Fu, W.M. Wang, R.Z. Yuan, Z.A. Munir, Int. J. SHS **2**, 307 (1993)
5 X. Zhang, X. He, J. Han, W. Qu, V.L. Kvalin, Mater. Lett. **56**, 183 (2002)
6 A.F. Fedotov, A.P. Amosov, Powder Metall. Met. Ceram. **41**, 7 (2002)
7 E.A. Olevsky, E.R. Strutt, M.A. Meyers, J. Mater. Process. Technol. **121**, 157 (2002)
8 M. Martinez Pacheco, E.P. Carton, M. Stuivinga, L. Katgerman, *Functionally Graded Materials* vol. VIII (Trans Tech, Aedermannsdorf, Switzerland, 2005), pp. 63–68
9 X. Zhang, J. Han, S. Du, J.V. Wood, J. Mater. Sci. **35**, 1925 (2000)
10 N. Sata, N. Sanada, T. Hirano, M. Niino, in *Combustion and Plasma Synthesis of High-Temperature Materials*, ed. by Z.A. Munir, J.B. Holt, VCH, New York 1990), p. 195
11 X. Ma, K. Tabihata, Y. Miyamoto, Ceram. Eng. Sci. Proc. **13**, 356 (1992)
12 I.-J. Shon, Z.A. Munir, J. Am. Ceram. Soc. **81**, 3243 (1998)
13 O. Schrott, Struers J. Materialogr. **40**, 6 (2003)
14 P.G. Slade, *Electrical Contacts, Principles and Applications* (Cutler-Hammer, Horseheads, New York, 1999), pp. 681–748
15 J.J. Moore, H.J. Feng, Prog. Mater. Sci. **39**, 275 (1995)